A plasmonic antenna-coupled superconducting near-IR photon detector

Faustin W. Carter,[1,*] **Daniel F. Santavicca,**[2] **and Daniel E. Prober**[1]

[1] *Yale University Applied Physics Department, 15 Prospect St., New Haven, CT 06511, USA*
[2] *University of North Florida Physics Department, 1 UNF Dr., Jacksonville, FL 32224, USA*

[*] *faustin.carter@yale.edu*

Abstract: The extremely small size of plasmonic antennas has made it difficult to integrate them with nanoscale detectors that require electrical leads, as the leads tend to degrade the resonant properties of the antenna. We present a design for integrating a plasmonic antenna with a nanoscale superconducting transition-edge sensor (TES) with electrical leads. Numerical simulations demonstrate high-efficiency coupling of 1550 nm incident photons into the sub-wavelength TES. Although we have chosen to design around a TES, this approach is broadly applicable to any dissipative nanoscale device that requires an electrical connection.

OCIS codes: (250.0040) Detectors; (220.2740) Geometric optical design; (250.5403) Plasmonics; (310.6628) Subwavelength structures, nanostructures; (310.6860) Thin films, optical properties.

References and links

1. G. Rebeiz, "Millimeter-wave and terahertz integrated circuit antennas," Proc. IEEE **80**, 1748–1770 (1992).
2. L. Novotny and N. van Hulst, "Antennas for light," Nat. Photonics **5**, 83–90 (2011).
3. P. Bharadwaj, B. Deutsch, and L. Novotny, "Optical antennas," Adv. Opt. Photonics **1**, 438–483 (2009).
4. W. Zhang, L. Huang, C. Santschi, and O. J. F. Martin, "Trapping and sensing 10 nm metal nanoparticles using plasmonic dipole antennas." Nano Lett. **10**, 1006–1011 (2010).
5. M. W. Knight, H. Sobhani, P. Nordlander, and N. J. Halas, "Photodetection with active optical antennas." Science **332**, 702–704 (2011).
6. L. Tang, S. E. Kocabas, S. Latif, A. K. Okyay, D.-S. Ly-Gagnon, K. C. Saraswat, and D. a. B. Miller, "Nanometre-scale germanium photodetector enhanced by a near-infrared dipole antenna," Nat. Photonics **2**, 226–229 (2008).
7. L. Novotny, "Effective wavelength scaling for optical antennas," Phys. Rev. Lett. **98**, 266802 (2007).
8. E. S. Barnard, T. Coenen, E. J. R. Vesseur, A. Polman, and M. L. Brongersma, "Imaging the hidden modes of ultrathin plasmonic strip antennas by cathodoluminescence." Nano Lett. **11**, 4265–4269 (2011).
9. A. Alu and N. Engheta, "Theory, modeling and features of optical nanoantennas," IEEE Trans. Antennas Propag. **61**, 1508–1517 (2013).
10. W. Zhang, H. Fischer, T. Schmid, R. Zenobi, and O. J. F. Martin, "Mode-selective surface-enhanced raman spectroscopy using nanofabricated plasmonic dipole antennas," J. Phys. Chem. C **113**, 14672–14675 (2009).
11. L. J. E. Anderson, E. Hansen, E. Y. Lukianova-Hleb, J. H. Hafner, and D. O. Lapotko, "Optically guided controlled release from liposomes with tunable plasmonic nanobubbles." J. Controlled Release **144**, 151–158 (2010).
12. A. G. Curto, G. Volpe, T. H. Taminiau, M. P. Kreuzer, R. Quidant, and N. F. van Hulst, "Unidirectional emission of a quantum dot coupled to a nanoantenna." Science **329**, 930–933 (2010).
13. R. W. Heeres, S. N. Dorenbos, B. Koene, G. S. Solomon, L. P. Kouwenhoven, and V. Zwiller, "On-chip single plasmon detection." Nano Lett. **10**, 661–664 (2010).
14. P. Fan, K. C. Y. Huang, L. Cao, and M. L. Brongersma, "Redesigning photodetector electrodes as an optical antenna." Nano Lett. **13**, 392–396 (2013).
15. K. Irwin and G. Hilton, "Transition-edge sensors," in *Cryogenic particle detection,* of *Topics in Applied Physics*, C. Enss, ed. (Springer Berlin Heidelberg, 2005), vol. 99, pp. 63–150.

#213044 - $15.00 USD Received 28 May 2014; revised 24 Aug 2014; accepted 26 Aug 2014; published 4 Sep 2014

16. A. Lita, A. Miller, and S. Nam, "Counting near-infrared single-photons with 95% efficiency," Opt. Express **16**, 3032–3040 (2008).
17. B. S. Karasik, S. V. Pereverzev, A. Soibel, D. F. Santavicca, D. E. Prober, D. Olaya, and M. E. Gershenson, "Energy-resolved detection of single infrared photons with $\lambda = 8$ μm using a superconducting microbolometer," Appl. Phys. Lett. **101**, 052601 (2012).
18. D. E. Prober, "Superconducting terahertz mixer using a transition-edge microbolometer," Appl. Phys. Lett. **62**, 2119–2121 (1993).
19. P. L. Richards, "Bolometers for infrared and millimeter waves," J. Appl. Phys. **76**, 1–24 (1994).
20. D. F. Santavicca, F. W. Carter, and D. E. Prober, "Proposal for a ghz count rate near-ir single-photon detector based on a nanoscale superconducting transition edge sensor," Proc. SPIE **8033**, 80330W (2011).
21. C. Brewitt-Taylor, D. Gunton, and H. Rees, "Planar antennas on a dielectric surface," Electron. Lett. **17**, 729–731 (1981).

1. Introduction

Efficient coupling of radiation into a sub-wavelength detector using an antenna is well understood at radio and microwave frequencies. These techniques have been extended to the THz domain by scaling down the antenna dimensions to the 100 μm range [1]. Unfortunately, this proportional scaling down of the antenna size no longer works at frequencies well above the THz. This is because metals no longer behave like good conductors near their plasma frequency ($\sim 3.57 \times 10^{15}$ Hz for aluminum). Recent research has begun to provide a theoretical framework and establish design rules for so-called optical antennas [2, 3]. These antennas operate by coupling incident radiation to collective electron oscillation modes called surface plasmons.

One such design is the plasmonic dipole [4–9]; it is analogous to the common radio dipole antenna, with two main differences. The first is that a radio dipole is designed to match the free-space wavelength of the radio signal, while a plasmonic dipole is designed to match the wavelength of a surface plasmon that is created by the incident free space radiation. The second is that plasmonic dipoles are much smaller than their radio and microwave counterparts, which makes attaching electrical leads (for reading out lower-frequency information such as rectified or mixed-down signals) problematic. The leads on a THz antenna can easily be made much smaller than the antenna in order not to disturb the antenna properties. However, plasmonic dipoles that resonate at optical frequencies (10^{14}–10^{15} Hz) are only a few 10s to a few 100s of nanometers in size, making the fabrication of nonperturbative electrical leads a significant challenge.

Because of their extremely small size and the difficulties inherent in fabricating leads, plasmonic antennas have been primarily utilized for measurements that do not require a direct electrical connection to the antenna. Examples include tip-enhanced Raman spectroscopy [10], attaching resonant nanoparticles to a macroscopic object in order to concentrate the field locally [11], coupling the emission of a quantum dot with a nano-antenna [12], and using plasmonic dipole antennas to increase the polarization-dependent light collection of a large-scale detector [5]. One notable exception is a paper by Tang et al. [6], where a germanium photodiode is placed at the feed gap of a plasmonic dipole antenna. Electrical leads are oriented perpendicular to the antenna, but they are larger than the size of the antenna and hence their effects cannot be neglected. Another configuration that has been demonstrated is that of terminating a plasmonic waveguide with a superconducting nanowire single-photon detector (SNSPD) to measure individual plasmons [13]. Although this is not an antenna (the detector is many times larger than the incident wavelength), it is a successful implementation of a plasmonic system delivering energy to a superconducting detector. Finally, an example of using metal electrodes to enhance optical absorption in a semiconductor nanowire photodetector was recently described by Fan et al. [14]

This paper presents a design for a plasmonic antenna that couples to a sub-wavelength detector while allowing a direct electrical connection to the detector — in our case, a supercon-

#213044 - $15.00 USD Received 28 May 2014; revised 24 Aug 2014; accepted 26 Aug 2014; published 4 Sep 2014

ducting transition edge sensor (TES). The TES exploits the temperature-dependent resistance of the superconducting phase transition to detect the energy of an absorbed photon [15]. The TES is biased and its resistance is monitored using electrical leads. Our design allows for the implementation of electrical leads that are simple to fabricate and do not compromise the plasmonic enhancement effects of the antenna. This design is broadly applicable to the integration of a plasmonic antenna with any dissipative nanoscale detector that requires an electrical readout.

The superconducting TES is the most sensitive energy-resolving single-photon detector demonstrated to date, with single-photon sensitivity into the near- and mid-IR [16, 17]. The intrinsic energy resolution (δE) of a superconducting TES scales as $\delta E \approx \sqrt{T^3 A}$, where T is temperature and A is device area. Thus, antenna coupling allows one to use a much smaller TES area compared to what is possible with regular optical coupling (where the device area is on the order of a few λ^2). Reducing the device size allows one to operate at a much higher temperature for a given δE. Recent work on TES detectors [16] for detecting near-IR photons used regular optical coupling, with TES area $A = 1600\ \mu\text{m}^2$, which can be compared to the area of the niobium (Nb) TES of Fig. 1, with $A = 0.065\ \mu\text{m}^2$. The sub-wavelength TES also allows for diffusion cooling, which achieves a much faster detector response [18] and hence a larger photon counting rate.

Efficient antenna-coupling to a sub-wavelength TES is well-established at THz frequencies [19], but has not been demonstrated at near-IR or optical frequencies. A calculation of the sensitivity, speed, and saturation threshold of a nanoscale TES has been done by Santavicca et al. for near-IR detection [20]. For a niobium detector element that is 325 nm long, 200 nm wide, and 16 nm thick with a superconducting critical temperature $T_c = 5$ K, the predicted response time is 107 ps and the predicted intrinsic RMS energy resolution is 0.44 eV. Here we present a scheme for achieving efficient coupling of 1550 nm near-IR photons to such a nanoscale TES.

2. Antenna design

2.1. Discussion

The traditional method for attaching a radio dipole antenna to a much smaller detector (a diode, for instance) is to place the detector at the small feed gap between two quarter-wavelength strips (or rods). This configuration results in a half-wavelength resonator with the detector at the current maximum. Optimal photon coupling is achieved when the antenna beam pattern efficiently couples to the input photon beam; if one uses very narrow leads to read out the lower frequency signal from the detector, the antenna characteristics will not be significantly perturbed. Unfortunately, this approach is not practical in the optical and near-IR regime due to fabrication challenges — the feed gap and lead widths would necessarily be on the order of a few tens of nanometers for an optical antenna. However, the basic idea of this design (detector at the central current maximum with leads designed to be non-perturbing at the input frequency) may be used to design a plasmonic version with one caveat: plasmonic systems use displacement current rather than current, and the input wavelength specified is that of a surface plasmon (λ_p) excited by the incident radiation rather than the free-space wavelength of the incident radiation itself (λ). For simplicity of discussion, the terms current and wavelength will continue to be used, but when they are applied to the plasmonic system it is the displacement current and plasmon wavelength that are being referred to.

For very small geometries it is advantageous from a fabrication standpoint to attach leads to the ends of the plasmonic dipole antenna, rather than at the center. Large-area leads placed at the ends function as a high-frequency ground, forcing the ends of the dipole antenna to be voltage nodes (current maxima). In order to place the detector at the center of the configuration and still have it at the point of maximum current, the half-wave dipole antenna must be lengthened in to a full-wave resonator by extending its length to $n\lambda_p$ where n is an integer.

#213044 - $15.00 USD Received 28 May 2014; revised 24 Aug 2014; accepted 26 Aug 2014; published 4 Sep 2014

In order to get the maximum voltage drop across the detector (thereby producing a large signal), the dissipative/non-linear portion of the detector should be half a wavelength long and extensions (made of the same metal as the large leads) should be added on either end of the dissipative/non-linear section to make the total length $n\lambda_p$. In simulations we have discovered that it is actually advantageous to choose $n = 2$ rather than $n = 1$ as it increases the coupling efficiency (discussed later). Figure 1 shows our design, which uses aluminum (Al) for the extensions and niobium (Nb) for the superconducting TES. The Al arms are thicker than the Nb TES to promote good step-coverage during fabrication. The ground pads are much thicker than the Al arms to force a voltage node (or zero electric field) at the interface between the Al arms and the ground pads. The total combined length of the structure between the large leads is $2\lambda_p$ (or, more properly, $3\lambda_p^{Al}/2 + \lambda_p^{Nb}/2$). The plasmon wavelength is longer in Al than it is in Nb, which is why each $3\lambda_p/4$ Al extension is more than 1.5 times larger than the $\lambda_p/2$ Nb section.

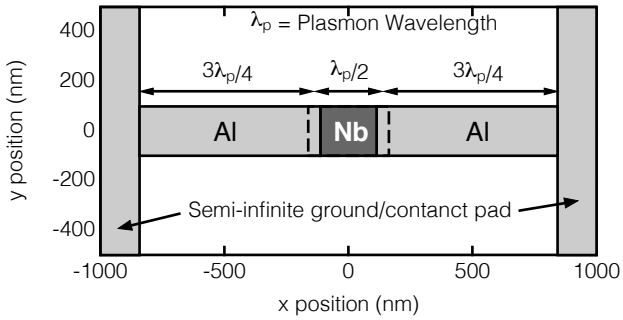

Fig. 1: Design for a TES coupled to a plasmonic resonator for 1550 nm photons. The total length of the resonator is twice the plasmon wavelength. The dashed lines indicate the Nb/Al overlap region, which is 50 nm long. The Nb element is 325 nm long, the Al elements are each 680 nm long.

2.2. *Calculation*

The length of a plasmonic dipole antenna does not scale linearly with the incident free-space photon wavelength. Instead, the relationship between the incident free-space wavelength (λ) and the resulting plasmon wavelength (λ_p) must be determined for each material at each incident wavelength. A theoretical treatment of the plasmonic dipole along with simplified antenna scaling rules has been developed by Novotny [7], and an alternate formulation exists by Barnard et al. [8]. A discussion of the theory behind the loading of plasmonic dipole antennas with various nano-loads is presented by Alu and Engheta [9]. A brief summary of the Novotny method (which we have used) follows: to begin, assume an infinitely long cylinder of radius R consisting of a metal embedded in a lossless dielectric with dielectric constant ε_s and wavenumber $k_s = \sqrt{\varepsilon_s}k_0$ where $k_0 = 2\pi/\lambda$. Let z be the direction of the rod axis. At near-IR and optical frequencies this metal rod will have a complex dielectric constant $\varepsilon(\lambda)$ with a negative real part (kinetic inductance) and a positive imaginary part (dissipation). If this rod is illuminated by radiation of wavelength λ polarized along its axis, one may deduce the modes that propagate down the rod in the z-direction by treating the rod as a waveguide and solving Maxwell's Equations The solution may be obtained by using separation of variables: the radial part of the modes in the rod are given by the cylindrical Bessel functions $J_n(\kappa_1 R)$, while the free-space fields are defined by cylindrical Hankel functions of the first kind $H_n^{(1)}(\kappa_2 R)$. The longitudinal part of the modes is sinusoidal and proportional to $\sin(2\pi z/\lambda_p)$, where λ_p depends on κ_1 and

#213044 - $15.00 USD Received 28 May 2014; revised 24 Aug 2014; accepted 26 Aug 2014; published 4 Sep 2014

κ_2 according to Eqs. (2) and (3). One may solve for the lowest order transverse magnetic mode (TM_0) by applying continuity of the logarithmic derivatives at the boundary of the metal rod to arrive at:

$$\frac{\varepsilon(\lambda)}{\kappa_1 R}\frac{J_1(\kappa_1 R)}{J_0(\kappa_1 R)} - \frac{\varepsilon_s}{\kappa_2 R}\frac{H_1^{(1)}(\kappa_2 R)}{H_0^{(1)}(\kappa_2 R)} = 0 \tag{1}$$

where κ_1 and κ_2 are given by:

$$\kappa_1 = k_0\sqrt{\varepsilon(\lambda) - \left(\frac{\gamma}{k_0}\right)^2}\ \kappa_2 = k_s\sqrt{\varepsilon_s - \left(\frac{\gamma}{k_0}\right)^2} \tag{2}$$

This mode corresponds to a surface plasmon excited by the incident radiation (polarized along z). One may solve this system of Eqs. for the propagation constant of the surface plasmon ($\gamma = 2\pi/\lambda_p$). Since we are interested here in the dispersion of the plasmon we take the real part of γ and then the surface plasmon wavelength is given by:

$$\lambda_p = 2\pi/Re[\gamma] - X \tag{3}$$

where X is a constant that depends on the geometry of the ends of the metal rod (since in any real-world problem the rod must be finite in length). For an infinite rod $X = 0$. For a finite length rod X is not trivial to calculate, but is easily determined by simulation. Truncating the cylinder so that its length corresponds to $\lambda_p/2$ establishes a resonant condition. The surface plasmon wavelength depends strongly on the dielectric constant of the metal rod, the surrounding dielectric, and the wavelength of the incident radiation.

Solving Eqs. (1) and (2) analytically is not possible in general. Novotny [7] presents a way to solve the equations for a number of limiting cases to arrive at a simple scaling law for plasmonic dipole antennas. However, it is straightforward to implement a numerical solution for λ_p, which may then be compared with simulations.

3. Simulation and results

3.1. Cylindrical Plasmonic Dipole Antennas

We have run simulations to determine λ_p for Nb using a commercial software package (CST Microwave Studio). The simulated geometry is a cylindrical metal rod with a radius of 20 nm and spherical end-caps. In these simulations it is assumed for simplicity that the value of the dielectric constant for the surrounding material is the average of the intended substrate and vacuum [21]. Each simulation followed a two step process. First, one illuminates a rod of length l (including end-caps) with plane waves (of varying wavelength), polarized along the rod, and calculates the absorption cross-section (σ_a) from the scattered fields. The longest wavelength λ at which σ_a is a maximum is the wavelength at which the metal cylinder has a dipole resonance, and so $\lambda_p = 2l$. This pair of numbers (λ, λ_p) generates a datapoint on the graph. Figure 2 shows a curve calculated from Eq. (3) fit to data from the simulations performed using CST. For this fit X was taken as a free parameter. In this plot the horizontal axis shows the free-space wavelength of the incident radiation and the vertical axis shows the corresponding plasmon wavelength for a Nb rod embedded in a vacuum-sapphire half-space. Sapphire was chosen as it has a relatively low dielectric constant in the near-IR ($\varepsilon = 3$), compared with other common substrate materials, thereby allowing for the largest possible antenna structure.

Both simulation and calculation require knowledge of the wavelength-dependent complex dielectric function $\varepsilon(\lambda)$ for thin-film Nb (not tabulated anywhere to our knowledge). To this end, we prepared a number of Nb thin films of varying thicknesses (8 nm–16 nm). The films

#213044 - $15.00 USD Received 28 May 2014; revised 24 Aug 2014; accepted 26 Aug 2014; published 4 Sep 2014

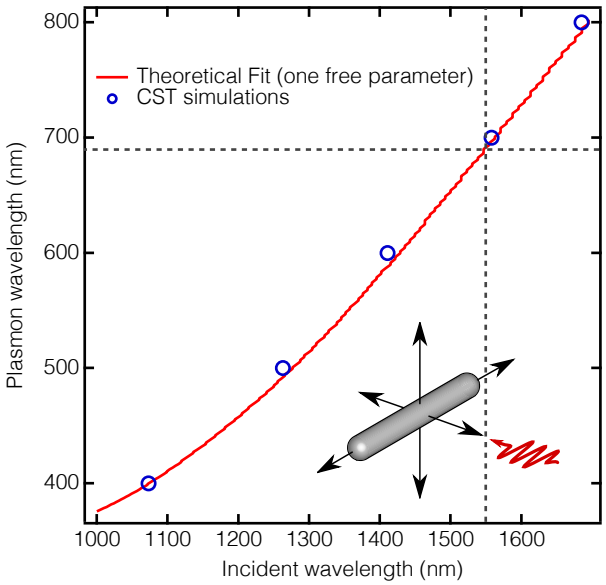

Fig. 2: Calculation of λ_p from Eq. (3) for cylindrical Nb nano rods with $R = 20$ nm and different lengths (solid line) has been fit to the results of CST simulations on the same geometry (open circles) with one free parameter ($X = 198$ nm). Inset depicts simulation geometry. Dashed lines indicate λ_p at 1550 nm.

were fabricated via electron-beam deposition of Nb onto room-temperature sapphire substrates. They were then sent to J.A. Woollam Co. where the complex index of refraction $n(\lambda) + ik(\lambda)$ was measured via spectroscopic ellipsometry for each Nb thickness; $\varepsilon(\lambda)$ was then computed from $n(\lambda)$ and $k(\lambda)$. Figure 3 shows the n and k data from J.A. Woolam for a Nb thickness of 16 nm. This thickness has a superconducting critical temperature (T_c) of approximately 7 K. The optical parameters of the other thickness films were qualitatively similar in shape, and differed by up to 10% in n and 20% in k at $\lambda = 1500$ nm.

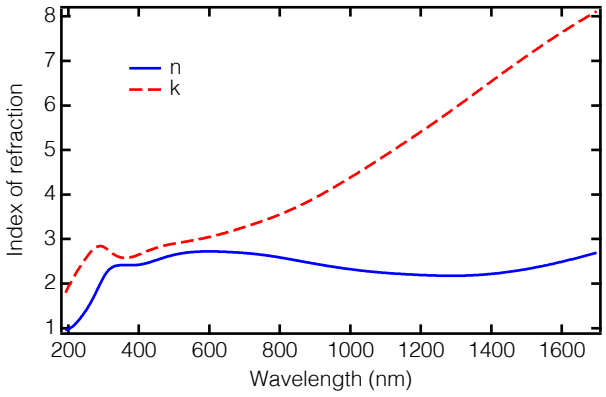

Fig. 3: Wavelength-dependent complex index of refraction for 16 nm thick Nb film.

We repeated this simulation for Al using book values for $\varepsilon(\lambda)$ of Al, but do not include

#213044 - $15.00 USD Received 28 May 2014; revised 24 Aug 2014; accepted 26 Aug 2014; published 4 Sep 2014

those results as they closely match those of Novotny [7]. A final caveat is that any real-world thin-film device will consist of a planar nanowire with a rectangular, rather than cylindrical, cross-section. Despite this difference, the analysis presented above works well for a planar nanowire provided one chooses an appropriate effective radius to plug into the calculation. The effective radius depends on the cross-sectional area of the nano-wire.

3.2. Full antenna-coupled detector design

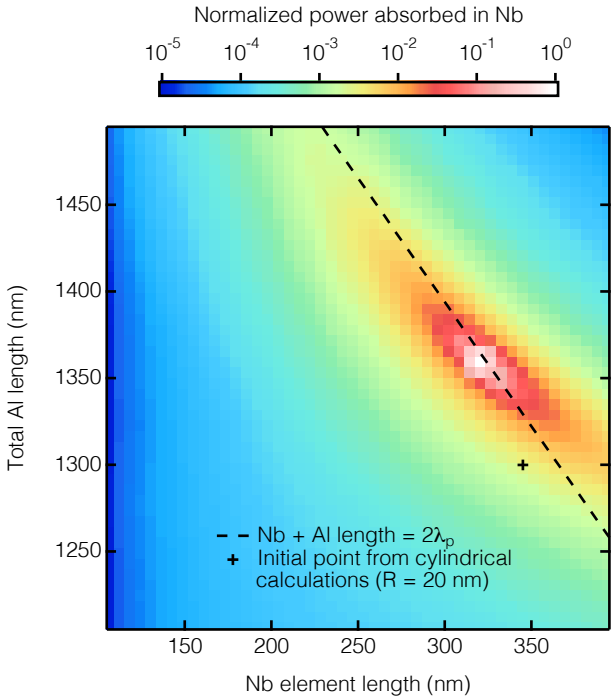

Fig. 4: Power absorbed in Nb detector (normalized to 1) as a function of both Al and Nb length, for $\lambda = 1550$ nm. The superimposed black line is a best fit to Eq. 4. The small cross indicates the initial parameters from the calculation of λ_p for Nb and Al cylinders with radii of 20 nm.

The results in Fig. 2 (and a similar calculation for Al) were used as initial parameters for determining the optimal length of the Nb and Al components of the design depicted in Fig. 1. We then performed a parametric analysis in Ansoft HFSS, a commercial high-frequency EM solver package. The Nb element is modeled as 16 nm thick, the Al extensions are 66 nm thick, and the large ground pads (the two leads) are 200 nm thick. The substrate is sapphire (rather, the surrounding dielectric is an average of vacuum and sapphire as in the previous section). The left, right, top, and bottom borders of the cell have periodic boundary conditions, and the two surfaces parallel to the page have what is called a radiation boundary; the program attempts to balloon them out to infinity. The bounding box was sized large enough that the periodic spacing of the antennas was sufficient to avoid any coupling between antennas. The Nb and Al lengths were treated as independent parameters. The simulation engine illuminated the structure with a 1550 nm plane wave polarized along the detector length and computed the power absorbed in the Nb element by integrating the Poynting vector $\vec{S} = (\vec{E}_i + \vec{E}_s) \times (\vec{H}_i + \vec{H}_s)$ (where "i" and "s" denote incident and scattered) over all surfaces of the Nb element. This was repeated for

#213044 - $15.00 USD Received 28 May 2014; revised 24 Aug 2014; accepted 26 Aug 2014; published 4 Sep 2014

a range of different Nb and Al lengths. The results of this parametric analysis are depicted in Fig. 4, where the x-axis is Nb length (l_{Nb}), the y-axis is Al length (l_{Al}), and the color of the points indicates the (normalized) power absorbed in the Nb detector element.

The dashed black line in Fig. 4 is a fit to:

$$\frac{l_{\mathrm{Nb}}}{\lambda_{\mathrm{p}}^{\mathrm{Nb}}} + \frac{l_{\mathrm{Al}}}{\lambda_{\mathrm{p}}^{\mathrm{Al}}} = 2 \tag{4}$$

where the fit parameters $\lambda_{\mathrm{p}}^{\mathrm{Nb}}$ and $\lambda_{\mathrm{p}}^{\mathrm{Al}}$ were calculated by assuming the maximum response corresponds to half of a plasmon wavelength in Nb, and three-quarters of a plasmon wavelength in each Al section (see Figs. 1 and 6). Equation (4) is predicated on the assumption that for any given Nb (or Al) length, the maximum response occurs when the total structure length is equal to two plasmon wavelengths. This naive model qualitatively matches the simulated response, however, the small deviation of the $2\lambda_{\mathrm{p}}$ line at longer Nb lengths indicates that a more complicated model is needed to fully explain the antenna response. The small cross in Fig. 4 indicates the starting point which was a result of calculations for a cylinder with a radius of 20 nm. This is remarkably close to the optimal value for the rectangular cross section (within 5%) and indicates that the cylindrical model is an excellent first approximation.

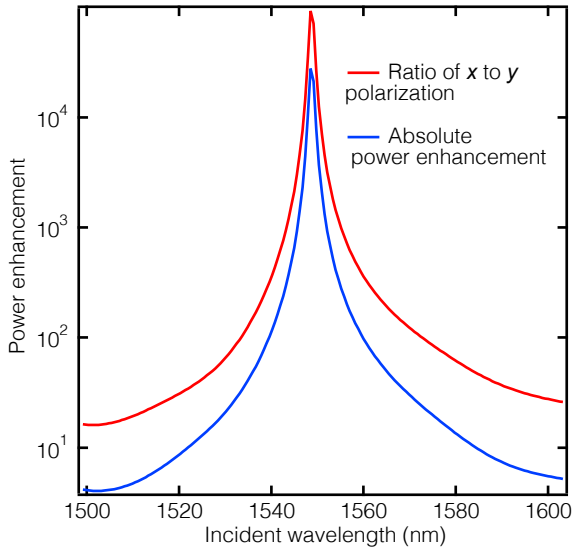

Fig. 5: Red: power absorbed in Nb element due to incident light polarized along the axis of the detector (x) normalized by power absorbed due to incident light polarized perpendicular to the detector axis (y). Blue: power absorbed in Nb element with aluminum antenna/leads normalized by power absorbed without any aluminum at all. Incident wavelength is free-space wavelength. See Fig. 1 for device design.

Figure 5 shows the simulated device response as a function of incident wavelength (computed by HFSS) for the optimal geometry as determined from Fig. 4 ($l_{\mathrm{Nb}} = 325$ nm, $l_{\mathrm{Al}} = 1360$ nm). The vertical axis is the ratio of power absorbed by the detector, normalized in two different ways. The top curve (red) is the ratio of power absorbed by the detector from light polarized parallel to the detector to power absorbed from light polarized perpendicular to the detector. The bottom curve (blue) is the absolute power enhancement; it is the ratio of power absorbed in the Nb with and without the Al antenna and ground pads. It is possible to tune the antenna

#213044 - $15.00 USD Received 28 May 2014; revised 24 Aug 2014; accepted 26 Aug 2014; published 4 Sep 2014

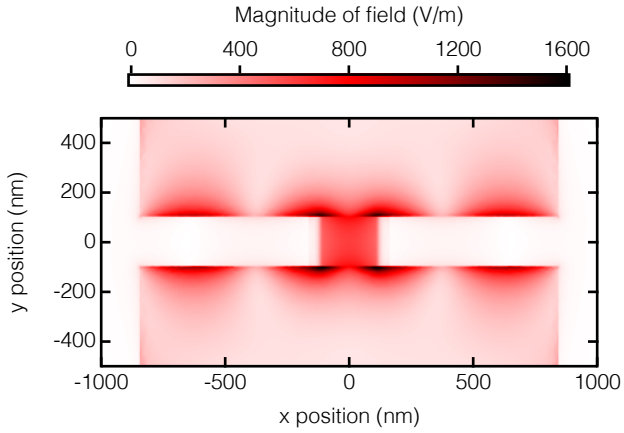

(a) Field Magnitude

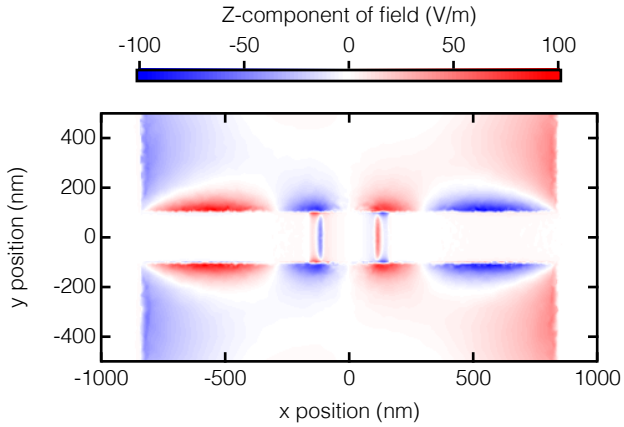

(b) Z-Component

Fig. 6: (a) Electric field strength at a height of 8 nm above the substrate (half the Nb height) superimposed on detector design (see Fig. 1) during illumination by 1550nm plane wave with field strength of 1 V/m. Note the strong field concentration at the detector, and the two-wavelength resonance (half a wavelength in the Nb, and three-halves in the Al). Also note the shorter plasmon wavelength in the Nb vs. the Al. (b) Z-component of field in same plane showing an unambiguous two-wavelength resonance.

to different wavelengths by rescaling all the dimensions according to the calculations above. The sensitivity of the resonance to variations in length can be seen from Fig. 4 and is within the accuracy limits of commercial electron-beam lithography technology. Further broadening of the peak is to be expected in any real-world implementation due to imperfections in the fabrication process, non-zero surface roughness, and possible defects in the thin films, which means the detector should still operate well at the designed wavelength with small fabrication errors.

Figure 6 depicts the electric field strength distribution at the resonance from Fig. 5 superimposed over the device. The resulting electric field is concentrated in and around the Nb detector element; it is roughly two orders of magnitude stronger in the Nb than in the Al. One can clearly

#213044 - $15.00 USD Received 28 May 2014; revised 24 Aug 2014; accepted 26 Aug 2014; published 4 Sep 2014

see the plasmon wavelength distribution (longer in the Al by a factor of about two), and count two full wavelengths. It is worth noting that because the plasmon wavelength is much shorter than the free-space photon wavelength, our $2\lambda_p$ design results in a device which is roughly 1.7 μm long and so nearly the same size as the photon it is designed to detect. Our simulations have shown much better coupling with the $2\lambda_p$ design compared to a resonator that is only one plasmon wavelength long between the ground pads. We believe this is because the large ground pads of the smaller device serve to reflect more of the incident free-space photons, whereas with the larger $2\lambda_p$ design, the gap between the pads is large enough to admit the photon to the device. This effect is one possible reason for the deviation of the response in Fig. 4 from the dashed line at smaller Al lengths.

4. Conclusions

We have developed an approach that allows integration of plasmonic antennas with nanoscale devices that require an electrical connection. Our design is tunable (through fabrication) and straightforward to fabricate using conventional electron beam lithography. The design's main advantage is that the leads do not negatively perturb the antenna resonance. A secondary advantage is that is naturally polarization sensitive. We demonstrate in our simulations that this approach should work well with a superconducting TES. In principle, this design could be extended to any small detector that requires an electrical connection, for example, a photodiode. As long as the antenna material (Al in our case) experiences much less dissipation than the detector (Nb in our case) at the resonant frequency, the power should couple strongly into the detector element.

Acknowledgments

The authors thank Prof. Nader Engheta for helpful conversations, and Dr. Mike Rooks and Dr. Luigi Frunzio for their advice on device fabrication methods and tolerances. D.S. acknowledges support from the National Aeronautics and Space Administration through the University of Central Florida's NASA Florida Space Grant Consortium (NNX10AM01H). F.C. acknowledges support from the NASA Connecticut Space Grant Consortium (NNX06AC32H). D.P. acknowledges support from the National Science Foundation (NSF) through the NSF-DMR-0907082 grant, and support from Yale University.

#213044 - $15.00 USD Received 28 May 2014; revised 24 Aug 2014; accepted 26 Aug 2014; published 4 Sep 2014